Science Advances

AAAS

advances.sciencemag.org/cgi/content/full/3/4/e1603119/DC1

Supplementary Materials for

Butterfly gyroid nanostructures as a time-frozen glimpse of intracellular membrane development

Bodo D. Wilts, Benjamin Apeleo Zubiri, Michael A. Klatt, Benjamin Butz, Michael G. Fischer, Stephen T. Kelly, Erdmann Spiecker, Ullrich Steiner, Gerd E. Schröder-Turk

Published 21 April 2017, *Sci. Adv.* **3**, e1603119 (2017)
DOI: 10.1126/sciadv.1603119

The PDF file includes:

Other Supplementary Material for this manuscript includes the following:
(available at advances.sciencemag.org/cgi/content/full/3/4/e1603119/DC1)

- movie S1 (.mov format). X-ray nanotomography.
- movie S2 (.mov format). Visualization of the chiral gyroid photonic crystal structure.

Supplementary Materials

Supplementary Text

Single-crystallinity and defect structure of individual gyroid crystallites

The crystallinity of the 47 reconstructed domains was inspected in slices through the reconstructed volumes (16-bit greyscale volumetric voxel data), orthogonally oriented towards the <100> and <111> directions of each individual domain, using the software Avizo for FEI Systems – Materials Science 8.1.0. In these slices, as exemplarily shown in fig. S6, characteristic periodic patterns of the chitin phase (brighter greyscale intensities) and the air phase (darker greyscale intensities) are observed. Irregularities in these patterns indicate photonic crystal defects.

For the vast majority (41 domains), each domain represented a single ordered gyroid crystal, without internal defects (fig. S6, left). Where two domains had grown to the point of touching each other, grain boundaries with defects occur. This is typically due to orientation mismatch between the individual, single-crystalline domains.

For the remaining 6 domains, we have observed internal defects within the crystallites (fig. S6, right). Four of these domains seem to be slightly bent, which caused the formation of few dislocations. Whereas the other two domains show a higher defect density, either due to a stronger bending or an orientation mismatch of two adjacent domains, which had grown together but cannot clearly be distinguished.

Crystallographic texture analysis

The three reconstructed tomograms were visualized using Avizo for FEI Systems – Materials Science 8.1.0 (volume and surface renderings). The orientations of average scale surface normals were determined by visual inspection. The orientations of the cubic basis vectors (<100> directions) of each of the 47 reconstructed domains were determined with respect to the scale surface normal. Therefore, each domain of the reconstructed tomograms was tilted along Tait-Bryan angles (so-called yaw angle and pitch angle in the scale coordinate system and roll angle in the domain coordinate system), which were directly obtained from the Avizo software. 14.9% of the observed domains had the <100> crystallographic direction aligned with the scale normal (to within 10°), 10.6% with the <110> direction and 2.1% with the <111> direction. The partial inverse pole figure in fig. S4 shows that the reconstructed domains exhibit a rather random orientation with respect to the scale surface normal.

Determination of the enantiomeric type

The <100> directions with four-fold symmetry and <111> directions with three-fold symmetry of each of the 47 domains were unambiguously determined by visual inspection in the 3D reconstructions using Avizo for FEI Systems – Materials Science 8.1.0 (volume and surface renderings). The domains with gyroid structure and cubic symmetry exhibit chiral channels with opposite handedness along its <100> and <111> directions. This knowledge was used to verify the crystal directions by tilting the domains into different <100> and <111> directions and checking the symmetry (three-fold or four-fold) and handedness (right-handed or left-handed); using the same handedness convention as in (*28*).

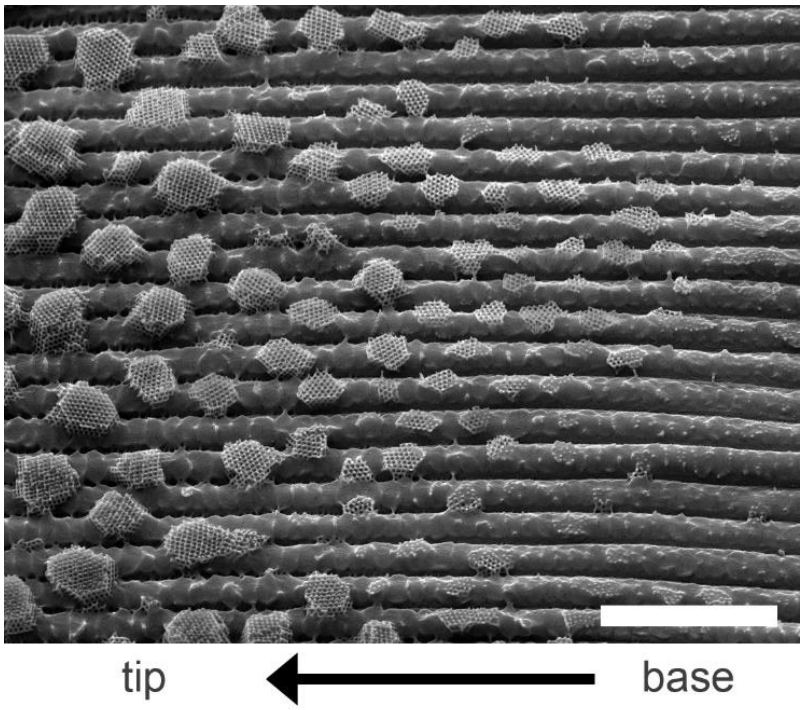

fig. S1. Gyroid nanostructures toward the base of the scales get smaller and less pronounced (scale bar, 10 µm).

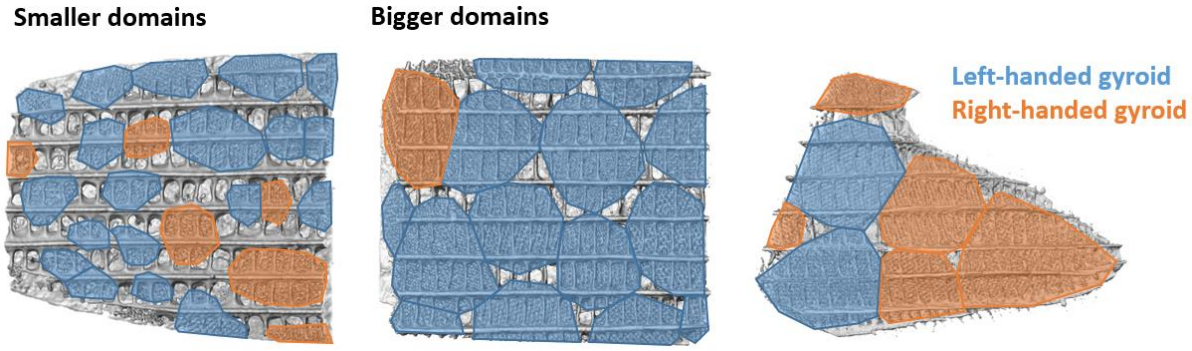

fig. S2. Handedness of the 47 gyroid crystallites determined in the three high-resolution x-ray nanotomography reconstructions. Left-handed gyroids (blue labels) clearly dominate. Note that the rightmost reconstruction is imaging a smaller scale volume compared to the other two reconstruction volumes (see also fig. S3).

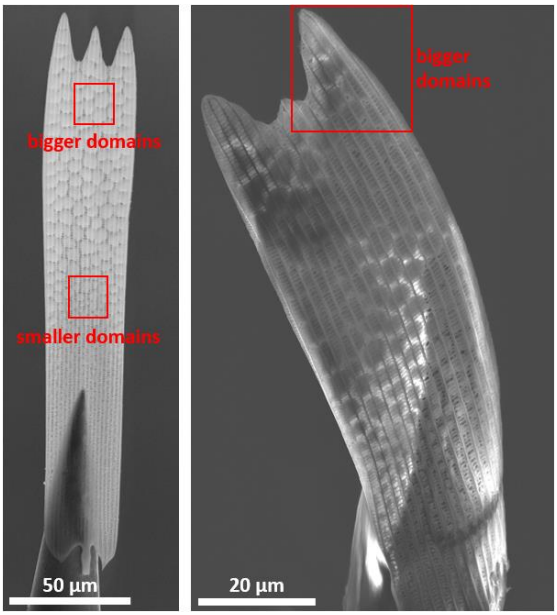

fig. S3. X-ray tomography samples. The two investigated butterfly wing scales glued to tungsten tips. The red rectangles mark the regions for the high-resolution X-ray tomography scans.

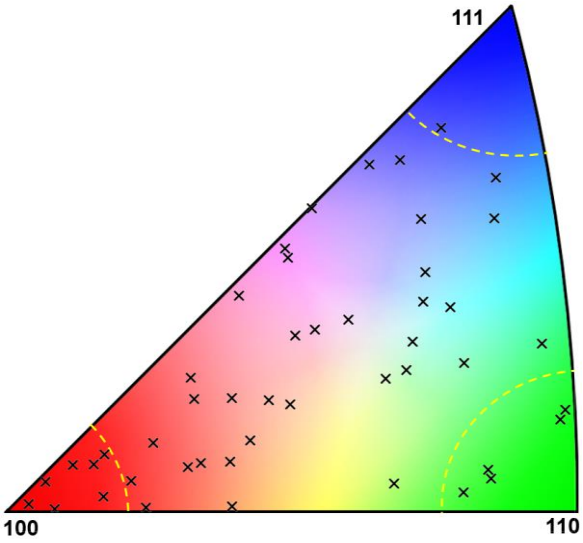

fig. S4. Orientation of crystallites. Partial inverse pole figure displaying the orientation of the scale surface normal with respect to the 47 reconstructed gyroid-structured crystallites (the dashed yellow lines indicate the regions around the poles within 10°). The orientation of the crystallites is random (c.f. (*14*, *28*) for results on *P. sesostris* and *C. rubi*).

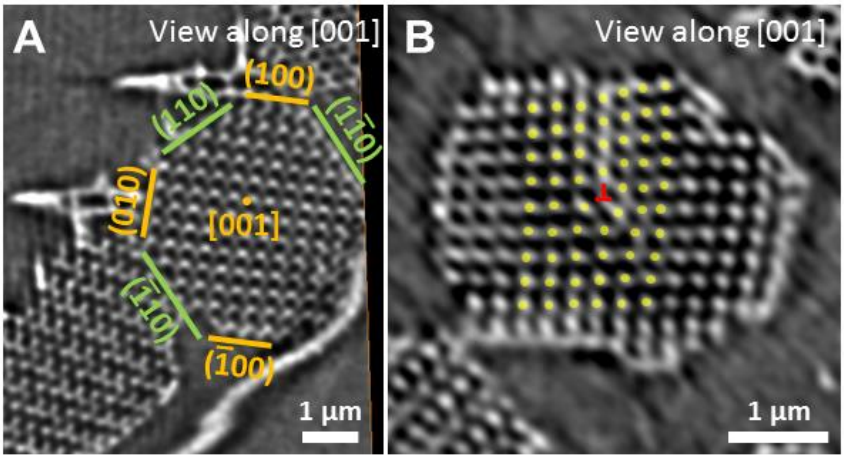

fig. S5. Crystallinity of gyroid crystallites. Exemplary slices through the 3D reconstructions perpendicular to low-order zone axes (e.g. [001]) show the single-crystallinity and faceted shape of the majority of the domains (**A**; identified crystal orientations and crystal planes are indicated). (**B**) Only a few domains exhibit internal defects (the identified dislocation core and the distorted cubic lattice positions are indicated).

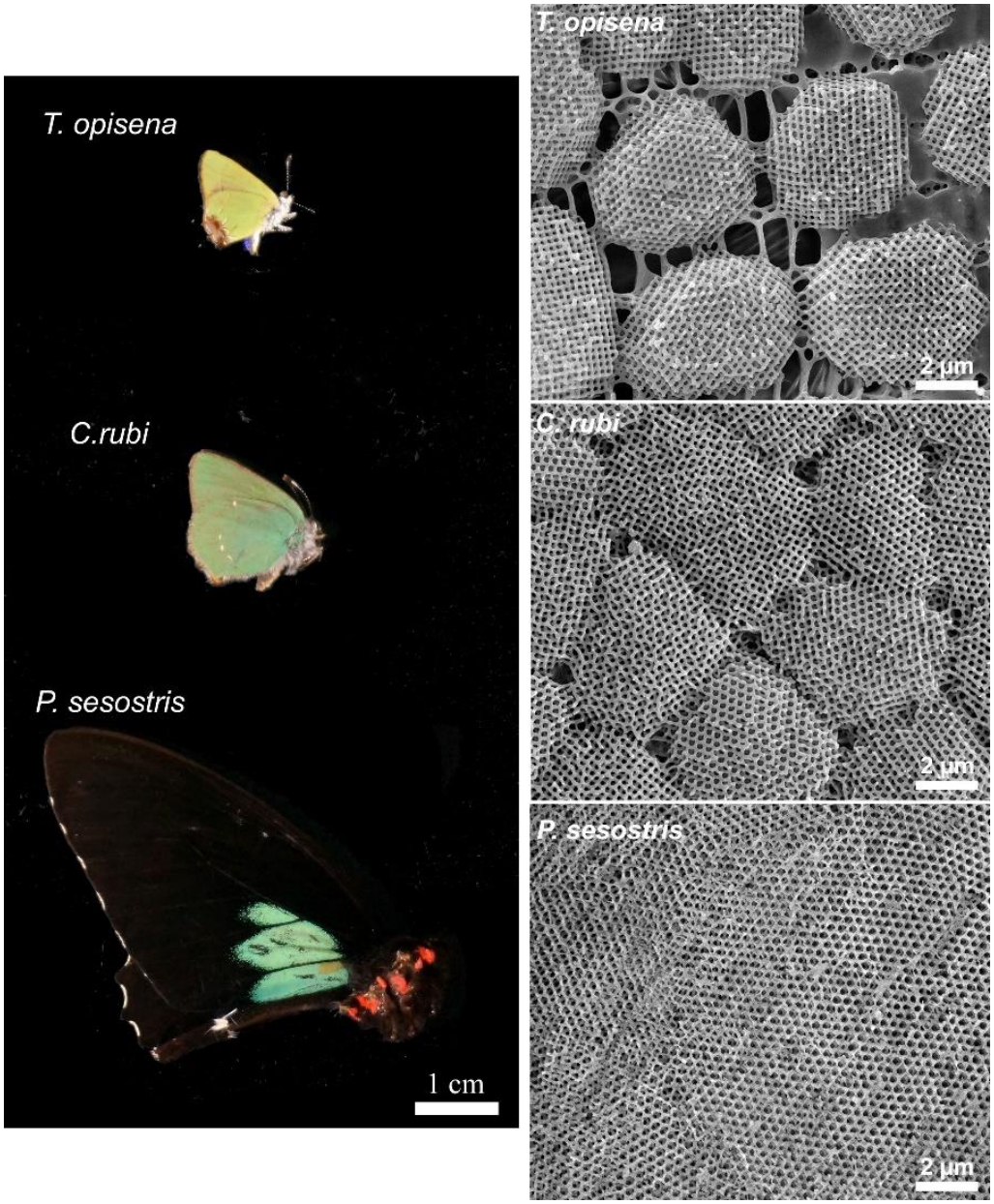

fig. S6. Comparison of the upside-down view of various gyroid-containing photonic structures of *T. opisena*, *C. rubi*, and *P. sesostris*. All these butterflies share a common cell-formation mechanism that seems to be stopped at different points in time: *T. opisena* (top) carries isolated gyroid crystallites (see also Figs. 2 and 5), whereas *P. sesostris* (bottom) has cover scales where the lumen is completely filled with gyroid crystallites. The development process in *C. rubi* (middle) seems to have stopped in-between.

Captions for Movies S1–S2

movie S1. X-ray nanotomography. Part 1: Tilt series in large field of view (LFOV) mode of the upper part of a single wing scale. Part 2: Slices through the reconstructed volume obtained from the LFOV tilt series seen perpendicular to the long axis of the scale moving towards the scale tip. Part 3: Tilt series in high resolution (HRES) mode of a region with larger domains (close to the tip of the scale from part 1). Part 4: Slices through the reconstructed volume obtained from the HRES tilt series seen perpendicular to the long axis of the scale moving towards the scale tip.

movie S2. Visualization of the chiral gyroid photonic crystal structure. Zoom into one exemplary bigger domain reconstructed by X-ray nanotomography in HRES mode (visualized by volume and surface rendering). The animation starts from a view perpendicular to the scale surface normal showing the complete reconstructed tomogram consisting of 15 distinct domains and then approaches one domain along one <111> direction with threefold symmetry. The photonic crystal exhibits a left-handed helix in the void domain along its <111> directions, which reveals a left-handed gyroid.